Article

pubs.acs.org/Biomac

Deconstructing a Plant Macromolecular Assembly: Chemical Architecture, Molecular Flexibility, And Mechanical Performance of Natural and Engineered Potato Suberins

Olga Serra,[†,‡] Subhasish Chatterjee,[†,§] Mercè Figueras,[‡] Marisa Molinas,[‡] and Ruth E. Stark*[,§]

[‡]Laboratori del Suro, Departament de Biologia, Universitat de Girona, E-17071, Girona, Spain

[§]Department of Chemistry, City College of New York, City University of New York, Graduate Center and Institute for Macromolecular Assemblies, New York, New York 10031, United States

Supporting Information

ABSTRACT: Periderms present in plant barks are essential protective barriers to water diffusion, mechanical breakdown, and pathogenic invasion. They consist of densely packed layers of dead cells with cell walls that are embedded with suberin. Understanding the interplay of molecular structure, dynamics, and biomechanics in these cell wall-associated insoluble amorphous polymeric assemblies presents substantial investigative challenges. We report solid-state NMR coordinated with FT-IR and tensile strength measurements for periderms from native and wound-healing potatoes and from potatoes with genetically modified suberins. The analyses include the intact suberin aromatic−aliphatic polymer and cell-wall polysaccharides, previously reported soluble depolymerized transmethylation products, and undegraded residues including suberan. Wound-healing suberized potato cell walls, which are 2 orders of magnitude more permeable to water than native periderms, display a strikingly enhanced hydrophilic−hydrophobic balance, a degradation-resistant aromatic domain, and flexibility suggestive of an altered supramolecular organization in the periderm. Suppression of ferulate ester formation in suberin and associated wax remodels the periderm with more flexible aliphatic chains and abundant aromatic constituents that can resist transesterification, attenuates cooperative hydroxyfatty acid motions, and produces a mechanically compromised and highly water-permeable periderm.

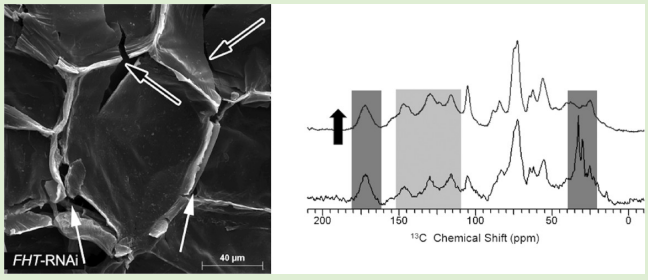

INTRODUCTION

Cork, technically designated as phellem, is the outermost tissue of the periderm, a complex dermal structure that replaces the plant epidermis in mature (secondary) organs such as tree trunks, roots and tubers, and healing tissues.[1] Cork works as an efficient barrier that protects the plant from dehydration and injuries. It is made of tightly packed dead cells evolved to fulfill two main requirements: to be impermeable to water and elastic enough to withstand mechanical stress. Cork hydrophobicity and mechanical resistance are attributed to the suberin macromolecule that is embedded within cork cell walls,[2,3] making an understanding of this composite material potentially useful for the design of analogous engineered polymeric materials.

The suberin polymer is comprised of aromatic and aliphatic domains linked via ester bonds.[4−7] Its aromatic lignin-like domain consists of a polymer made from monolignols and hydroxycinnamic (mostly ferulic) acids and derivatives; this domain is thought to be covalently bound to primary cell-wall polysaccharides.[8,9] The aliphatic domain is a biopolyester that upon transesterification releases mainly soluble C_{16}−C_{28} ω-hydroxyacids and α,ω-diacids but also fatty acids and primary alcohols, glycerol, and small amounts of ferulic acid.[10] Deposited between the primary wall and the cell plasma membrane, the aliphatic domain forms a polymeric matrix in which a mixture of extractable lipids (associated waxes), most related to suberin monomers, is dispersed. Under the electron microscope, the aliphatic matrix with embedded waxes appears as a multilamellar stack indicative of a highly organized macromolecular assembly.[11] Substantial residues that resist saponification, which broadly speaking are designated as suberan, have also been reported in suberized tissues.[8,12−14] They represent a portion of the suberin macromolecular assembly containing aliphatic and aromatic constituents and covalently linked polysaccharides.

Although extensive compositional information is available for suberin, its macromolecular organization[7,15] and interactions with other cell-wall polymers[6] are still far from being understood. A central challenge for the molecular characterization of cell-wall biopolymers involves focusing on the material of interest without compromising its inherent molecular structure. The suberin information obtained by

Received: November 3, 2013
Revised: February 2, 2014
Published: February 6, 2014

dx.doi.org/10.1021/bm401620d | Biomacromolecules 2014, 15, 799−811

GC-MS is limited to the portion of the polymer susceptible to breakdown and is largely confined to identification of monomeric fragments. Solid-state nuclear magnetic resonance (ssNMR), which can elucidate the functional groups and cross-link sites within intact polymers,[16−18] provides a complementary investigative route. For instance, previous ssNMR studies have yielded important structural information on cutin, the cell wall biopolyester in the epidermis of leaves, young shoots, and fruits.[16,19−22] Information derived from ssNMR has also been reported on suberin from industrial cork[23−26] and from potato tuber periderm. Whereas most studies of potato suberin by ssNMR and FT-IR methods have used the wound periderm,[9,27−31] recently the native tuber periderm has also been investigated.[13,32,33] The two types of periderm are similar in relative aliphatic suberin composition[34,35] but differ significantly with respect to the aromatic products resulting from thioacidolysis[36] and have permeabilities to water that span 2 orders of magnitude.[34] By considering the respective intact polymers, soluble depolymerization products and undegraded residues in concert, a more comprehensive understanding of suberin should be available.

Targeted genetic engineering, which can be applied to specifically modify individual polymers without damaging the structural integrity of the cell wall, is a powerful tool for the investigation of plant macromolecular assemblies. Recently, potato lines with genetically modified suberin were generated by RNA interference (RNAi)-mediated gene silencing: StKCS6, involved in aliphatic chain elongation;[37] CYP86A33, responsible for the ω-hydroxylation of fatty acids; and FHT, necessary for the formation of suberin alkyl ferulates.[38] These studies revealed significant changes in suberin composition and ultrastructure but also in periderm texture and water barrier properties (Table 1). The availability of these modified potato periderms for ssNMR analyses, supported by FT-IR and tensile strength, offers exciting new prospects for determining how the molecular interactions ultimately control the viscoelastic properties and permeability of the cork cell walls.

Table 1. Summary of Functional Properties, Ultrastructure, and Transesterification Products for Genetically Modified Native Periderms as Compared with Wild-Type

name	native periderm ultrastructure, waterproofing, and chemical composition[a]
wild-type	smooth periderm
StKCS6-RNAi[38]	smooth periderm, retained lamellar ultrastructure
	1.5-fold increased permeability
	−75% > 26 - carbon depolymerization products (fatty acids, alcohols)
CYP86A33-RNAi[45]	thinner suberin layer, lost lamellar ultrastructure
	3.5-fold increased permeability
	−43% aliphatic depolymerization products, −54% 18:1 ω-hydroxy fatty acid, −86% 18:1 α,ω-diacid
FHT-RNAi[39]	russeted dark tan periderm; retained lamellar ultrastructure
	15-fold increased permeability
	−62% aliphatic depolymerization products, −89% ferulates, −89% 18:1 ω-hydroxyfatty acid, −71% primary alcohols

[a]Calculated as μg of suberin mg^{-1} dry periderm (see Table S1).

MATERIALS AND METHODS

Plant Material. Wild-type and genetically modified potato plants (*Solanum tuberosum*) used in this work were from cv Desirée. The plants were propagated in vitro, transferred to soil and greenhouse grown to obtain tubers as described by Serra et al.[37] For all experiments, two lines corresponding to two different previously characterized transformation events were used for each genetic modification (StKCS6-RNAi, lines 5 and 34; CYP86A33-RNAi, lines 22 and 39; FHT-RNAi, lines 4 and 37). Tomato exocarp was prepared as described previously.[45]

Suberin-Enriched Periderm Membranes. The native periderm was collected from mature tubers stored at room temperature for 21 days after harvest. The periderm of the tubers (peel) was separated using a potato peeler and the phellem or cork layer isolated using an enzymatic mixture. To remove unsuberized tissue, the peels were shaken at 150 rpm with 2% (v/v) *Aspergillus niger* cellulase (MP Biomedicals, Illkirch, France) in a 50 mM pH 5.0 acetate buffer, for 48 h each at 37 and 44 °C, respectively. Subsequently, the peels were treated with 2% (v/v) *A. niger* pectinase (Sigma, St. Louis, MO) in a pH 4.0 acetate buffer, for 24 h each at 28 and 31 °C, respectively. Sodium azide (Sigma, St. Louis, MO) was added at 1 mM final concentration to inhibit bacterial growth. Then the isolated periderm membranes, comprising exclusively the suberized cell walls of the phellem (cork) layer of the periderm, were washed with deionized water and dried at 35 °C. Although only the suberized phellem tissue is obtained whereas the phellogen and phelloderm are digested during the enzymatic treatment, we use the term periderm instead of phellem following a number of prior authors.[30,39,40]

The wound periderm was obtained from healing potato discs 7 days after wounding. The discs were prepared by sectioning the potato flesh tissue from 7-month old tubers with a mandolin slicer and left to heal on wet cellulose filter paper placed on a wire netting inside plastic boxes that contained water at the bottom to maintain humidity. The brown layer of wound periderm on the surface was collected by blade peeling at 7 days as described previously.[41] Removal of unsuberized tissues was conducted enzymatically as described above.

Wax-free periderm membranes were obtained by Soxhlet extraction under reflux conditions using three successive solvents of varying polarity, methanol, chloroform, and hexane, for 24 h each. The resulting suberin-rich wax-free periderms were used for ssNMR analysis on intact suberin; FT-IR experiments were performed on both undewaxed and wax-free materials.

Undegraded Suberin Residue from Depolymerization. The residues were obtained from wax-free periderm membranes by incubation for 18 h at 70 °C with 10% (v/v) boron trifluoride in methanol (BF_3; Fluka, St. Louis, MO) to achieve polymer degradation by transesterification.[42,43] These protocols have been validated extensively.[29,40,44]

Solid-State NMR Spectroscopy. Compositional analyses of periderms were made from solid-state NMR spectra. Analogously to experiments reported for tomato fruit cutins,[45] magic-angle spinning ^{13}C NMR data were collected on 2−5 mg of powdered plant material with a Varian (Agilent) VNMRS NMR spectrometer equipped with a 1.6 mm FastMAS probe operating at a typical spinning speed of 10 or 15 kHz (±20 Hz). The ramped-amplitude cross-polarization magic-angle spinning experiments (CPMAS) were conducted with a spin-lock/cross-polarization (CP) time of 1−2 ms, a 10−20% linear ramp of the ^{1}H field strength during cross-polarization, and a 3 s recycle delay between successive acquisitions so as to identify carbon-containing functional groups via their respective chemical shifts. In addition, CPMAS ^{13}C experiments with a 10 kHz spinning rate and interrupted proton decoupling for periods of 10−40 μs prior to signal acquisition were conducted to suppress signals from carbons relaxed by attached hydrogens, while retaining nonprotonated and mobile carbon moieties.[46,47] Direct-polarization experiments (DPMAS) using a 100 s recycle delay provided relative proportions of each carbon moiety via integration of specified spectral regions. The SPINAL method[48] was used to implement high-power heteronuclear proton decoupling, achieving ^{1}H field strengths corresponding to 170−185 kHz in separate experiments. Detailed experimental parameters for both CPMAS and DPMAS measurements have been reported elsewhere.[45,49,50]

The spectral data were typically processed with 100−200 Hz line broadening and analyzed in parallel using VNMRJ (version 2.2C; Agilent Technologies, Santa Clara, CA) and ACD/NMR Processor Academic Edition (version 12; Advanced Chemistry Development, Inc., Toronto, ON, Canada, www.acdlabs.com, 2013). Chemical shifts were referenced externally to the methylene ($-CH_2-$) group of adamantane (Sigma-Aldrich) at 38.48 ppm. Integrated signal intensities were measured using both cut-and-weigh methods and Photoshop software, designating the following chemical shift ranges for each major structural grouping: alkyl chains (8−50 ppm); alkoxy groups (50−92 ppm); arenes and alkenes (92−160 ppm); carboxyl groups (160−185 ppm). Experimental error limits for the compositional analyses (10−15%) were evaluated by repeating the DPMAS measurements at two different values of ^{1}H decoupling power; biological error limits (∼15%) were established from experiments on replicate periderm samples, as described previously for tomato fruit cuticles.[45]

Molecular flexibility assessments were made by several methods. The fraction of "liquid-like" $(CH_2)_n$ groups was estimated for each potato periderm sample by comparison of DPMAS NMR signal intensities with low-power (∼5 kHz) and high-power (∼175−180 kHz) ^{1}H decoupling. The rapid ($\sim 10^8-10^9$ s^{-1}) and slow ($\sim 10^5$ s^{-1}) motions were each assessed at several carbon sites of the wild-type native and wound periderms using solid-state NMR spin relaxation experiments. Traditional ^{1}H rotating-frame relaxation times that allow for abundant-spin diffusion, $\langle T_{1\rho}(H)\rangle$, were measured from the decay of carbon signal intensities with ^{13}C−^{1}H contact time in a CPMAS experiment.[51] Site-specific rotating-frame relaxation times, $T_{1\rho}(H)$, for each ^{1}H nucleus directly bonded to an observed ^{13}C nucleus, were measured with a Lee−Goldburg (LG) spin lock and LG cross-polarization period to suppress ^{1}H spin diffusion;[52,53] the experiments used a short 0.5 ms LGCP time and included 62−106 kHz LG pulses in separate trials. The LGCP experiments were also conducted rotor asynchronously. The latter spin relaxation experiment was validated by comparison with published results for crystalline alanine (Sigma-Aldrich).[54,55] To determine the carbon spin−lattice relaxation times $T_1(C)$, the recovery of ^{13}C signal intensity was monitored following cross-polarization with a 2 ms contact time and inversion of the signal.[56] All relaxation measurements were conducted at a spinning speed of 10 kHz (±20 Hz) and a nominal set temperature of 25 °C. Both $T_1(C)$ and $T_{1\rho}(H)$ relaxation data were fit using Origin software (OriginLab, Northampton, MA); for each carbon peak, the relaxation curve obtained using maximal peak height was fit by a single-exponential function.[57,58]

FT-IR Analysis. Spectra were measured with either of two instruments equipped for Attenuated Total Reflection (ATR) analyses: a Satellite FT-IR spectrometer (Mattson Instruments, Madison, WI; Specac, Slough, England) or a Nicolet 380 Smart MIRacle FT-IR spectrometer (Thermo Electron Corporation, Madison, WI) for undewaxed and dewaxed periderms, respectively. Undewaxed periderm samples were enzymatically isolated membranes, with measurements made for four individual wild-type tubers and four individual FHT-RNAi tubers (two from line 4 and two from line 37). Dewaxed periderm samples were powdered material prepared for the NMR experiments. Spectra were recorded between 4000 and 550 cm^{-1}, with resolution of 4 cm^{-1} and 16 scans per sample (undewaxed), 2 cm^{-1} and 64−128 scans (dewaxed). For spectral comparisons, multiple-point baseline correction including local minima around 4000, 3700, 3000, 2700, 1800, 1700, 1485, 1190, 775, and 630 cm^{-1} was performed in conjunction with spectral normalization following Zeier and Schreiber.[59] Band integration of each spectrum was conducted using eFTIR software (Essential FTIR, http://www.essentialftir.com/index.html). The aliphatic (CH_2) and aromatic (C=C) stretching regions were roughly integrated in the ranges 2990−2815 and 1700−1480 cm^{-1}, respectively.[13]

Tensile Strength and SEM Analysis. Undewaxed native periderm membranes were hydrated by soaking in water for 1 h, then cut into narrow strips 5 mm in width and 15 mm in length. The strips were mounted in a dynamic mechanical analyzer (DMA, Mettler Toledo DMA/SDTA 861e, Columbus, OH) and held by grips exposing a 5.5 mm length of periderm strip. Then the periderm was pulled to increase the tension at a constant rate of 0.11 mm min^{-1} until failure produced two broken fragments. The broken fragments were fixed under vacuum with 4% formaldehyde in pH 7.5 phosphate-buffered saline at room temperature for at least 48 h. Then, they were dehydrated with an increasing ethanol concentration series, exchanged through amyl acetate and critical-point dried. The pieces were mounted on copper stubs and coated with gold. Two replicates of each were obtained for StKCS6-RNAi (line 34), CYP86A33-RNAi (line 22), FHT-RNAi (line 37), and wild-type periderms. Specimens were observed using a Zeiss DSM 960A scanning electron microscope (SEM; Zeiss, Oberkochen, Germany). Digital images were collected and processed using Quartz PCI 5.10 software (Quartz Imaging Corporation, Vancouver, Canada).

RESULTS

1. Molecular Structures of Suberin in Native versus Wound Periderms. The molecular composition and structure of suberin were compared for wild-type wound and native periderm samples. Cross-polarization magic-angle spinning (CPMAS) ^{13}C NMR was first used to establish the reproducibility of data collected on nominally identical samples and to make a rapid qualitative assessment of the chemical moieties present in each periderm type. Figure 1 shows representative spectra of the intact suberin in native and wound dewaxed periderms. A high degree of similarity was established among biological replicates (Figure S1); reproducibility of the spectroscopic results was also verified by duplicate measurements on the same sample at two different spinning speeds (10 and 15 kHz). In spite of the observation of relatively broad resonances,[12] the resolution of the high-field spectra was sufficient to allow provisional identification of numerous carbon types by reference to previously published reports. These assignments are summarized in Figure 1 and Table S2.

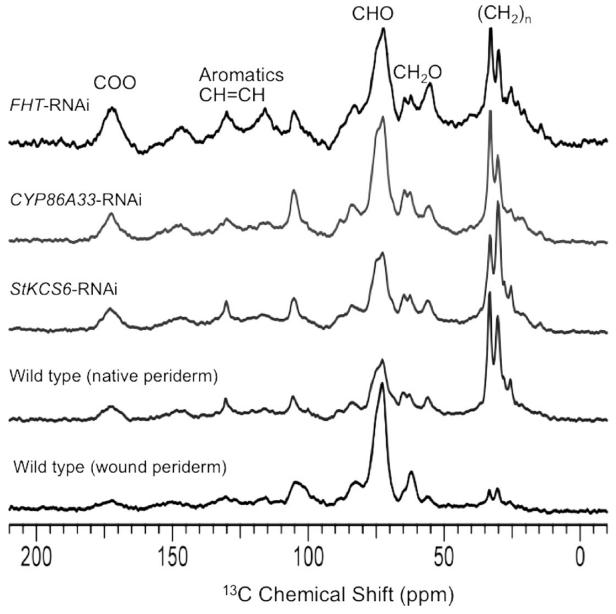

Figure 1. CPMAS ^{13}C NMR (150 MHz) of wax-free wild-type and genetically modified (RNAi) native and wound periderms, showing analogous aliphatic-aromatic polyester functional groupings in different proportions. Quantitatively reliable ratios of different carbon types were obtained from analogous DPMAS spectra.

As expected for a chemically heterogeneous aliphatic-aromatic polyester, the intact suberin in both native and

wound periderms exhibits broad spectral features and displays resonances attributable to long-chain aliphatics (centered at 25−33 ppm), alkenes and aromatics (120−160 ppm), and carboxyl groups (170−173 ppm).[27] Both materials show characteristic resonances from polysaccharide cell walls and/or other CHO and CH_2O moieties (62−101 ppm) and the CH_3O groups typical of guaiacyl and sinapyl hydroxycinnamic acid moieties. These resonance assignments were also confirmed in native periderm using delayed decoupling experiments,[46] which distinguish rigid protonated carbons from nonprotonated and relatively mobile functional groups[27] (Figure S2).

Despite the observation of comparable CPMAS resonances indicating a common set of carbon-containing moieties, quantitatively reliable direct-polarization magic-angle spinning (DPMAS) ^{13}C NMR experiments revealed notably different relative amounts of the principal structures in intact suberins from native and wound periderms (Figure 2). The latter

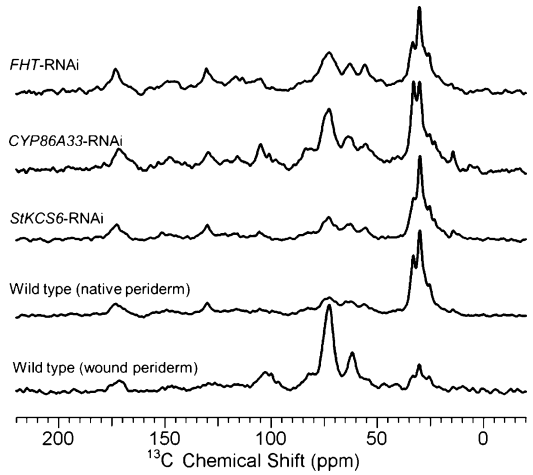

Figure 2. DPMAS ^{13}C NMR (150 MHz) of wax-free wild-type and genetically modified (RNAi) native periderm and wound periderm, used to determine ratios of carbon types within each spectrum.

measurements are essential for amorphous materials: their comparatively mobile segments cross polarize inefficiently and are thus undercounted in the traditional CPMAS spectrum, whereas their most rigid molecular moieties will display broadened resonances if the ^1H decoupling field is too small. Although quantitative comparisons *between* spectra of different materials may also be compromised by instrumental variations or uncertainties in mass, the relative ratios *within* each spectrum permit reliable and informative compositional comparisons.[60] The DPMAS spectra and integrated areas of key spectral regions reveal, most strikingly, that intact suberin in native periderm has a greater relative number of chain methylene groups (8−50 ppm) with respect to multiply bonded (92−160 ppm), oxygenated aliphatic (50−92 ppm), and COO (160−185 ppm) moieties (Figure 3). Viewed from the perspective of the $(CH_2)_n$ groups that are expected to associate strongly with waxes to form a waterproofing layer, a progressively increasing proportion of alkyl chain content is observed in potato wound periderm, then native periderm, and finally tomato fruit cutin.[18,45,49,61] Conversely, the polysaccharide- and polyester-derived alkoxy carbons outnumber the $(CH_2)_n$ groups in wound-healing tissues.

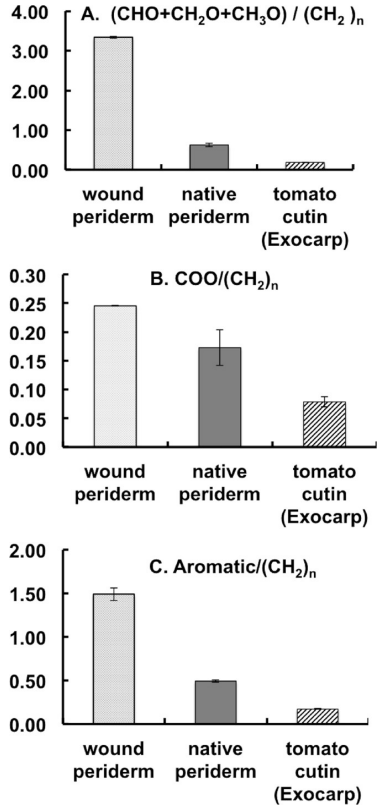

Figure 3. Ratios of carbon-containing functional groups in potato periderms and tomato fruit cuticles, derived from DPMAS ^{13}C NMR spectra obtained at an operating frequency of 150 MHz. Detailed procedures and error limits are described in the Materials and Methods.

2. Molecular Structures of Suberin in Genetically Modified Native Potato Periderm. Intact suberin in native periderm from potatoes that are genetically modified to alter the biosynthesis of specific suberin structures (Table 1; see Table S1 for comparative chemical composition of depolymerization products) was analyzed and compared with wild-type native and wound periderms. Figure 1 shows CPMAS ^{13}C NMR spectra of StKCS6-RNAi, CYP86A33-RNAi, and FHT-RNAi intact suberins compared with that of wild-type. Biological replicates of the RNAi-silenced plants, including two independent transformation lines for each down-regulated gene, yielded highly reproducible NMR spectra (Figure S3). For these intact suberins, our CPMAS spectra and delayed decoupling results (Figure S2) showed that each genetically modified macromolecular assembly contains the same chemical groups, but the spectra also provided preliminary indications of their notably different relative NMR signal intensities and corresponding functional group proportions.

Quantitative analysis of the corresponding DPMAS spectra yields the ratios shown in Figure 4, which compare the amounts of each structural element to the long-chain methylene groups. Figure 4A shows that the ratios of alkoxy carbons (from the suberin polyester and associated cell-wall polysaccharides) to $(CH_2)_n$ groups rise to 2.2 and 1.6 times their wild-type values in CYP86A33-RNAi and FHT-RNAi intact suberins, respectively. Figure 4B shows a qualitatively similar trend for carboxyl groups as compared with long-chain aliphatics, including progressive increases for StKCS6-RNAi, FHT-RNAi, and CYP86A33-RNAi intact suberins. Both of these compositional

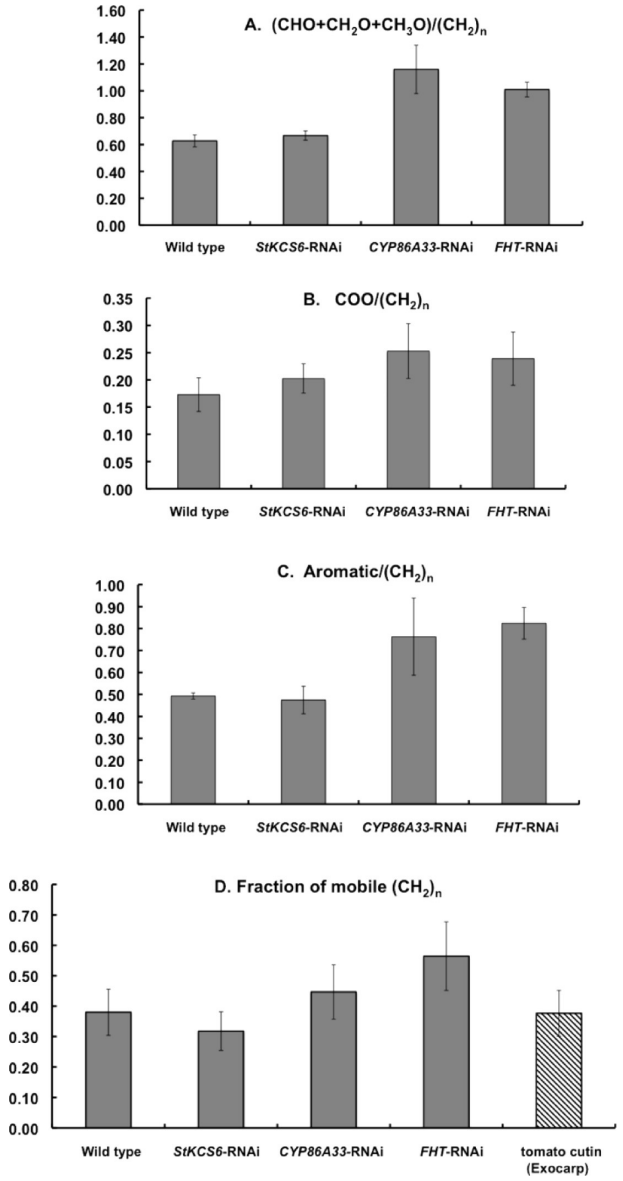

Figure 4. Ratios of carbon-containing functional groups and fractions of mobile long-chain methylene groups in native periderms from wild-type and genetically modified plants, and fractions of mobile long-chain methylene groups in tomato cutins, derived from DPMAS ^{13}C NMR spectra obtained at an operating frequency of 150 MHz.

trends indicate an enhanced hydrophilic−hydrophobic balance and parallel the findings of prior chemical analyses conducted for soluble depolymerization (transesterification) products (Table 1). That is, for intact suberins from FHT-RNAi and CYP86A33-RNAi periderms, the relative reduction in $(CH_2)_n$ groups is reasonable because the amounts of the predominantly fatty acid and fatty alcohol product mixtures drop to 38−57% in those two downregulated lines; conversely the amounts of the intact StKCS6-RNAi suberin products are nearly identical to the wild-type periderm.

In an analogous manner, Figure 4C illustrates the similarity in relative amounts of aromatics and alkenes with respect to $(CH_2)_n$ groups for StKCS6-RNAi intact suberin compared to the wild-type, but also a nearly 2-fold increase for the CYP86A33-RNAi and FHT-RNAi suberins. It should be noted that in our quantitative estimates the resonances between 92 and 160 ppm are considered as a group, although qualitative differences are observable among the native periderm spectra displayed in Figure 2, especially for the FHT-RNAi. For CYP86A33-RNAi, this observation parallels the prior transesterification results, which show lesser reductions in aromatic breakdown products than either fatty acids or alcohols.[44] Thus, the sharp reduction of fatty acid and alcohols along with their $(CH_2)_n$ groups could contribute to this relative increase in aromatics. The augmented aromatic content of FHT-RNAi compared with wild-type is also supported by FT-IR spectra of the periderms (Figure S4), albeit with a larger degree of variability among undewaxed biological replicates. These latter spectra display notably enhanced ratios of stretching bands attributable to phenolic acids and aromatics conjugated with C═C moieties (1700−1480 cm^{-1}) with respect to aliphatic chain CH_2 groups (2990−2815 cm^{-1}),[13] in addition to hydrogen-bonded OH groups (3356 cm^{-1}) attributable to both polyesters and waxes; measurements for dewaxed periderms (Figure S4) were largely consistent with the NMR-derived compositional trends for native and wound periderms. The augmented prevalence of arenes and alkenes for the FHT-RNAi periderm, which may appear surprising in light of notably reduced ferulates found among the corresponding soluble transesterification products,[38] is addressed below in terms of possible structural changes within the aromatic suberin domain. Nonetheless, delayed decoupling ^{13}C CPMAS spectra for both native FHT-RNAi and wild-type periderms (Figure S2) yield CH/C estimates (0.5−0.7) indicative of predominantly sinapyl and guaiacyl phenolic units, as reported previously for wild-type potato wound periderm.[9]

3. Molecular Structures of Undegraded Residues versus Intact Suberins. In order to obtain a more reliable and comprehensive view of the molecular constituents of the periderm biopolymers, soluble depolymerization products and insoluble depolymerization residues were considered in concert. The CPMAS spectra in Figure 5A show a native periderm residue that demonstrates significant removal of the aliphatic chain moieties (∼25−35 ppm) and multiply bonded functional groups (110−150 ppm), in agreement with prior reports.[13,33] Consistent data are obtained for replicate biological samples, with the trends confirmed quantitatively by DPMAS spectral acquisition (Figure S5). The preferential retention of rigid $(CH_2)_n$ resonances at 33 ppm, reported recently for river birch (*Betula nigra*) bark suberan,[14] was not observed for these undegraded suberin residues. The removal of most aliphatic chain moieties from the insoluble polymer composite is expected in light of the abundant 18:1 ω-hydroxyacids and α,ω-diacids reported among the soluble transesterification products, but the retention of significant peak intensity in the COO region (∼172 ppm) could be attributable to aliphatic esters or polysaccharide uronic acids[62] that can possibly resist this depolymerization treatment.

For the corresponding wound suberin shown in Figure 5B, long-chain aliphatics contribute modestly to the spectrum of the intact suberin and are further diminished in the undegraded residue, following the same qualitative trend as native suberin (Figure 5A) and as reported previously.[12] In addition to retention of the carboxylates, the aromatic resonances are largely retained in the solid-state ^{13}C NMR spectrum of the undegraded wound suberin residue (Figure 5B).

The recalcitrant residues from native wild-type, StKCS6-RNAi, CYP86A33-RNAi, and FHT-RNAi suberin each display ^{13}C NMR spectra with attenuated $(CH_2)_n$ NMR signals and

dx.doi.org/10.1021/bm401620d | *Biomacromolecules* 2014, 15, 799−811

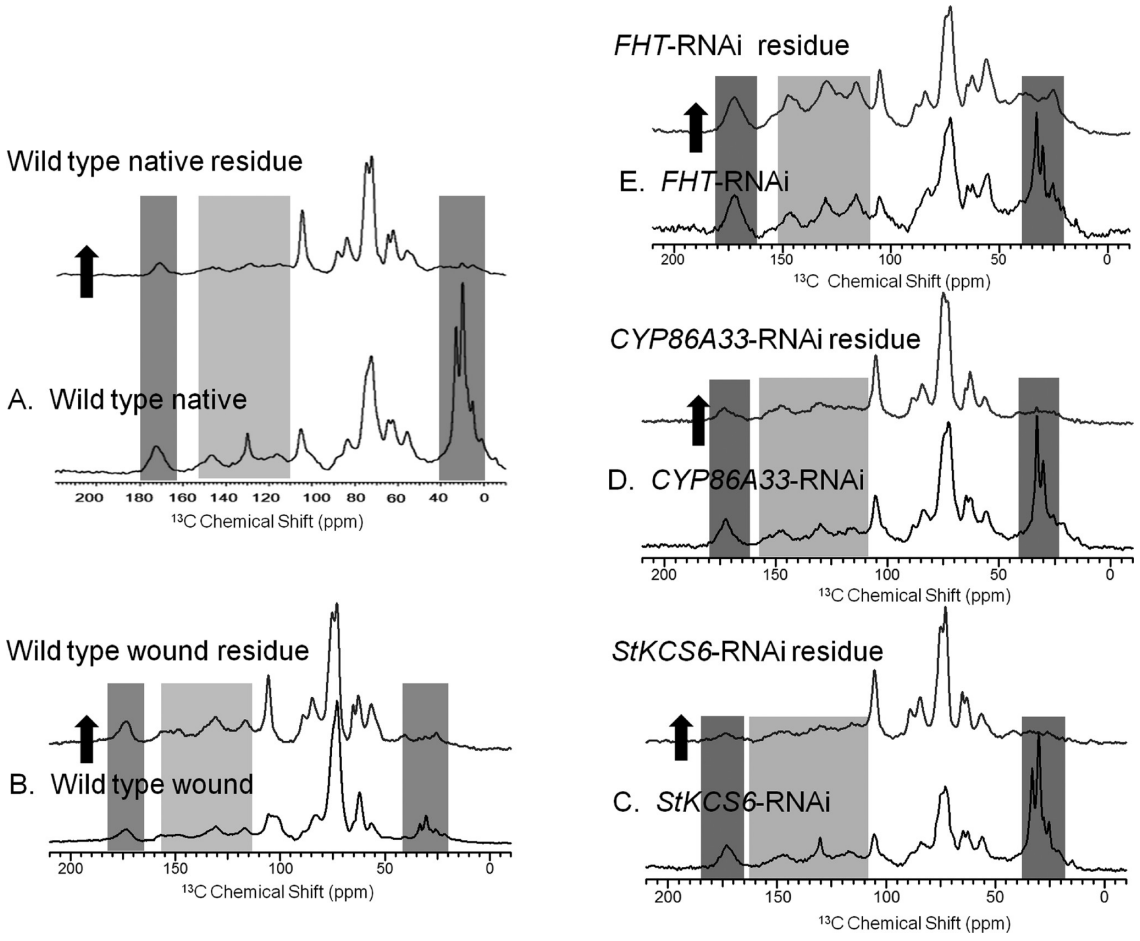

Figure 5. CPMAS ^{13}C NMR (150 MHz) spectra of wild-type and genetically modified native periderms and their undegraded solid residues after methanolysis.

prominent oxygenated aliphatic carbon resonances. For the StKCS6-RNAi (Figure 5C) and CYP86A33-RNAi (Figure 5D), aromatic constituents are nearly gone and carboxyl signals are partially attenuated as described for the native wild-type residue. Finally, Figure 5E shows significant signal intensity remaining in all regions of the ^{13}C NMR spectrum for the FHT-RNAi suberin residue. Whereas for wild-type, StKCS6-RNAi, and CYP86A33-RNAi the undegraded residues are dominated by alkoxy carbon resonances attributable primarily to polysaccharides, the FHT-RNAi residue maintains a suberin-like character: carboxyl, arene, and alkene moieties are evident as is a broadened distribution of chain-methylene resonances. This substantial retention of aromatic resonances supports significant contributions of the aromatic suberin domain to the high aromatic content found in FHT-RNAi intact suberin (Figure 4C) and is in accord with the qualitative spectral variations noted between 92 and 160 ppm (Figure 2).

Taken together, these findings directly demonstrate the efficacy of chemical hydrolysis for esters located putatively in the aliphatic domain of wild-type, StKCS6-RNAi, and CYP86A33-RNAi periderms. Moreover, the substantial spectral features in the chemical shift range between 60 and 180 ppm indicate oxygenated aliphatics, multiply bonded moieties, and carboxylates retained in the undegraded solid residue and support the preservation of both polysaccharides and an aromatic suberin domain that are architecturally inaccessible to hydrolytic attack and/or rich in other nonhydrolyzable structures. For FHT-RNAi periderms, however, the retention of significant ^{13}C NMR signal intensity in all spectral regions is an unexpected finding.

4. Site-Specific Flexibility and Overall Periderm Resilience: Rapid Local Motions and Cooperative Slow Motions. As noted previously, the significant differences in permeability and resistance to infection of protective plant coverings are expected to reflect their supramolecular architectures, intercomponent packing efficiencies, and cracking tendencies.[22,28,37,38,44,61,63−66] Thus, measurements of alkyl chain flexibility were undertaken as a proxy for periderm resiliency and a prelude to tests of mechanical performance.

The fraction of "liquid-like" aliphatic chains in the wild-type native and genetically modified periderms was estimated by comparing DPMAS ^{13}C NMR signal intensities of the mobile portion (low-power ^{1}H decoupling) with the entire $(CH_2)_n$ population (high-power decoupling). These measurements report on the prevalence of rapid local segmental motions at resonance frequencies of $\sim 10^8-10^9$ s^{-1}. Roughly 35−40% of the chain methylenes are highly mobile for both wild-type and StKCS6-RNAi periderms (Figure 4D), tracking their similar alkoxy-to-bulk methylene ratios and hydrophilic−hydrophobic balance (Figure 4A,B). These mobile fractions match reports for tomato cutin,[61] but they are double the values obtained for potato wound periderm using a different analytical protocol.[28] By contrast, although the FHT-RNAi and CYP86A33-RNAi chain methylenes are diminished in number compared with

other structural moieties (Figure 4A–C), ~50–60% of them have "liquid-like" flexibility in the context of solid-state NMR (Figure 4D). Comparative flexibility assessments of the cross-polarizable chain methylenes were also obtained from the delayed decoupling spectra (Figure S2), for which signal intensities of rigid protonated carbons are suppressed but mobile protonated carbons are preferentially retained together with nonprotonated carbons if $^{1}H-^{13}C$ dipolar interactions are partially averaged by molecular motion. Both mobile and rigid alkyl chain components (30 and 33 ppm, respectively) appear in wild-type as well as in all of the genetically modified periderms, most prominently in the CYP86A33-RNAi periderm for which lamellar structure is absent.

For the major "solid-like" (comparatively rigid) carbon fractions that can be cross polarized in ^{13}C NMR experiments, spin relaxation measurements were used to compare flexibility within the aliphatic domain for wild-type (native and wound) and FHT-RNAi periderms. Figure 6 summarizes the spin–

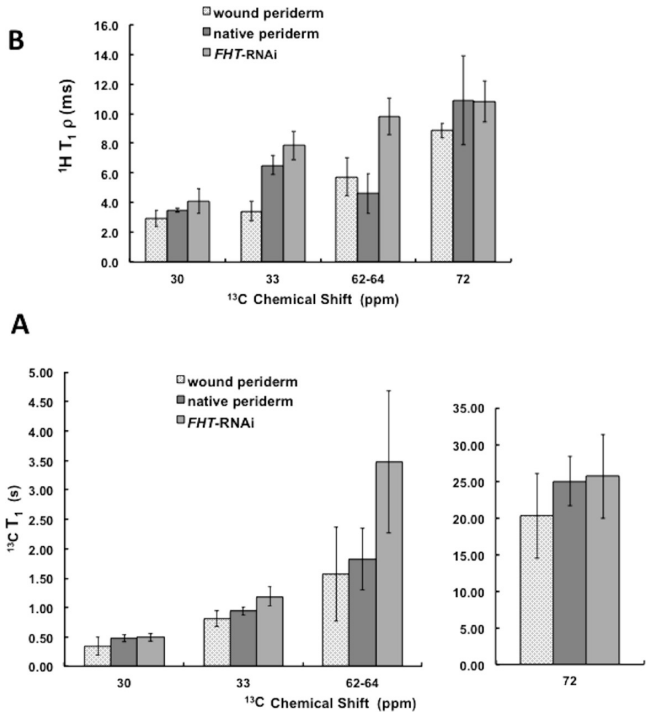

Figure 6. NMR spin relaxation times for native and wound-healing wild-type (Desirée) potato periderms. (A) ^{13}C spin–lattice relaxation times, $T_1(C)$, for functional groups including long-chain aliphatics (30 and 33 ppm), CH_2O (62–64 ppm), and CHO (72 ppm). (B) Rotating-frame spin relaxation times, $T_{1\rho}(H)$, measured using an ~90 kHz Lee–Goldburg (LG) spin-lock field via the respective attached carbons with chemical shifts as noted above. Additional measurements with a LG spin-lock field of ~106 kHz are shown in Figure S6.

lattice relaxation time $T_1(C)$ values that reflect nanosecond segmental molecular flexibilities (~10^8–10^9 s^{-1}) across the spectrum of molecular sites and have been related to the bulk modulus and other mechanical properties of solid polymers.[67] Each periderm exhibits efficient local motion (short spin–lattice relaxation times) for $(CH_2)_n$ groups (30 and 33 ppm) but substantial rigidity for CH_2O groups (62–64 ppm) and CHO (72 ppm) moieties. These site-specific variations are in accord with prior spin relaxation measurements for wound periderm.[28] Among the $(CH_2)_n$ resonances, noticeably longer values of $T_1(C)$ (fewer nanosecond motions) are also evident at the 33 ppm carbon sites in each sample, for which environmental and motional variations have been taken to indicate proximity to polyester–polysaccharide anchoring sites[24,28] or ordered aliphatic suberan chains that resist chemical depolymerization.[14] As deduced above from the DPMAS spectra that report on all carbons in the periderm samples, the cross-polarizable carbon fraction at 33 ppm has lengthened values of $T_1(C)$ that are indicative of more rigid aliphatic chains; this trend is especially pronounced for FHT-RNAi (Figure 6). On the other hand, the primarily polysaccharide moieties (62–64 and 72 ppm) exhibit moderately diminished local flexibility (longer values of $T_1(C)$) for both the native wild-type and FHT-RNAi with respect to wound periderm samples (Figure 6).

Finally, wild-type and FHT-RNAi native and wound periderms were compared in terms of the slower microsecond cooperative molecular motions (~10^5 s^{-1}) that have been correlated with impact strength or toughness in synthetic polymers.[68] Contrary to the trends observed for $T_1(C)$, Figure 6B reveals fewer microsecond molecular motions (longer values of $T_{1\rho}(H)$) for alkyl chain sites (30 and 33 ppm) in the native wild-type and FHT-RNAi periderms compared to wild-type wound periderm. The disparity in rotating-frame spin relaxation times that reflect collective motions is particularly clear for the semicrystalline 33 ppm $(CH_2)_n$ groups. The CH_2O (62–64 ppm) and CHO (72 ppm) moieties, which are largely retained in the undegraded residues and primarily polysaccharide in character, reorient similarly on this slower (microsecond) time scale in wild-type native and wound periderms; FHT-RNAi exhibits relatively higher $T_{1\rho}(H)$ values indicating somewhat less efficient motions for CH_2O groups that are retained preferentially with respect to CHO moieties in the undegraded residue spectrum (Figure S5). Taken together, the spin relaxation data demonstrate flexibility variations that depend on the periderm sample, which time scale is probed, and which polymeric constituent is considered.

5. Mechanical Performance of Genetically Modified Periderm Membranes. Genetically modified potato plants provide effective investigative probes of the individual contributions of the suberin components to the mechanical performance of the periderm. Therefore, uniform strips of undewaxed wild-type and genetically modified periderms were subjected to tensile strength challenges by pulling at a constant rate until failure using a dynamic mechanical analyzer. Once broken, the strips were inspected at their surfaces and fracture sites by SEM (Figure 7).

When subjected to tension, the periderm strips from StKCS6-RNAi behaved similarly to wild-type, while those from CYP86A33-RNAi and FHT-RNAi showed lower strain capacity (54 and 72%, respectively) and failed at lower loads. Microscopic inspection of wild-type periderm (Figure 7A,B) showed good dimensional recovery of the cells after stress relief. A similar recovery was observed for StKCS6-RNAi periderm (Figure 7D,E). In contrast, CYP86A33-RNAi and FHT-RNAi showed incomplete recovery with some breakage of their surfaces. After stress relief, the CYP86A33-RNAi periderm strips displayed a more folded appearance at the cell edges, with breakages occurring mostly along the cell walls by cell edges (Figure 7G,H, white arrows). Because unsuberized cell walls were removed by cellulase and pectinase before making these measurements, this CYP86A33-RNAi breakage behavior may indicate thinner and more heterogeneous suberin walls. Finally, FHT-RNAi strips showed breakages with straight edges that

dx.doi.org/10.1021/bm401620d | Biomacromolecules 2014, 15, 799–811

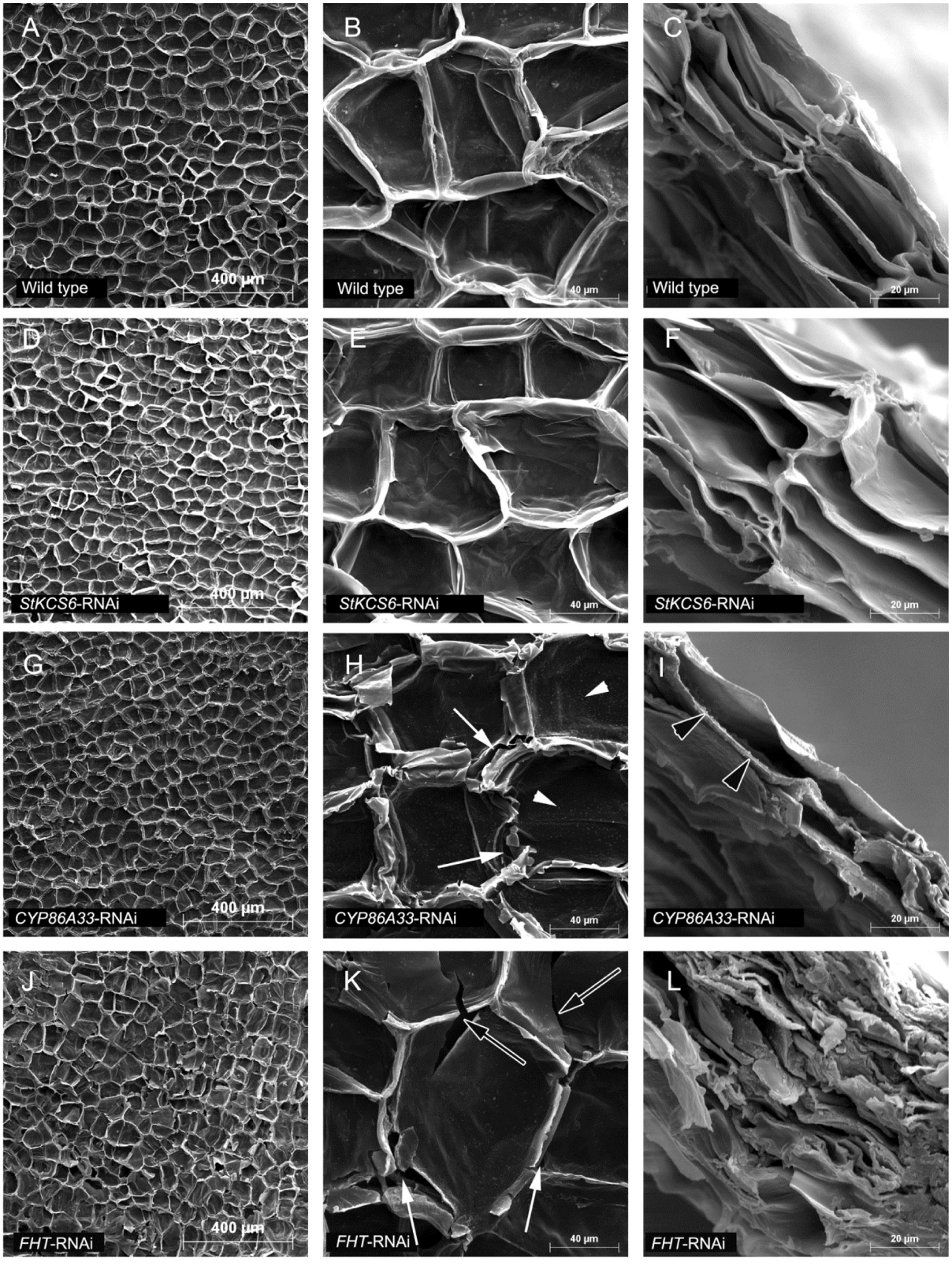

Figure 7. SEM images of native periderm membranes isolated from wild-type and genetically modified potatoes observed after tensile breaking stress: (A–C) wild-type periderm; (D–F) StKCS6-RNAi periderm; (G–I) CYP86A33-RNAi periderm; (J–L) FHT-RNAi periderm. The inner surface strained periderm (left column), its magnification (center column), and the fracture site (right column) are shown. White arrows indicate fissures along cell walls by cell edges that are abundant in the CYP86A33-RNAi periderm (H) and black-filled arrows fissures across cell walls typical of FHT-RNAi periderm (K). Note the abundant wax granules in the internal surface (H, arrowheads) and the indentation of the cross-sectioned cell walls at the site of fracture of the CYP86A33-RNAi periderm (H).

dx.doi.org/10.1021/bm401620d | *Biomacromolecules* 2014, 15, 799–811

were mostly across the cell wall surface (Figure 7J,K, black arrows), suggesting a stiffer cell wall material.

Upon inspection of the cross sectioned cell walls at the fracture site, again StKCS6-RNAi showed no differences from wild-type (Figure 7C,F); both materials displayed thin and smooth cell walls. For CYP86A33-RNAi, cross-sectioned cell walls exhibited characteristic indentations (Figure 7I, black arrowhead), suggesting a grained disposition of the suberin in accordance with the altered ultrastructural lamellation of this periderm (Table 1). However, it should be noted that in this case a number of wax granules deposited on the cell wall surface (Figure 7H, white arrowhead) may mask the image of the wall sections. As previously described (Table 1) the FHT-RNAi periderm is much thicker than wild-type as it accumulates more phellem cell layers, which are found to be collapsed in the tension-fractured periderm strips (Figure 7L).

DISCUSSION

1. Critical Evaluation of the Investigative Approach. An important goal at the outset of the current study was the rigorous validation of solid-state ^{13}C nuclear magnetic resonance (ssNMR) and FT-IR as reliable, nondestructive spectroscopic techniques that can probe the macromolecular organization of suberin−polysaccharide cell wall composites in plant periderms comprehensively. Likewise, the current study confirms the use of genetically modified suberins as an effective tool to elucidate the fundamental basis for their micromechanical and physiological properties.

All native, wound, and genetically modified suberins show the functional groups typical of a suberized tissue[9,21,23,24,27,69] in their CPMAS ^{13}C NMR spectra (Figure 1), and this conclusion is supported by complementary FT-IR data for wild-type and FHT-RNAi samples (Figure S4). Biological replicates demonstrate the excellent reproducibility of the NMR spectroscopic results, indicating the robustness of the analyses (Figures S1 and S3). For instance, CPMAS spectra of the native potato periderms (cv. Desirée) show dominant peaks assigned to aliphatic chains at 30 and 33 ppm, followed by intense resonances from the polysaccharide and polyester-based alkoxy carbons (Figure 1); wound periderms displayed the aliphatic chain features (0−45 ppm) but with diminished intensity. The DPMAS NMR spectra, though requiring substantial acquisition times, provide quantitative estimates of carbon-based molecular composition that are representative of the entire polymer composite (Figure 2).

Finally, spin relaxation data supplement determinations of the type and relative number of functional groups with site-specific assessments of molecular flexibility on contrasting and complementary time scales. The motional parameters have well-established links to the mechanical properties of diverse synthetic and natural polymer composites.[70] For instance, local segmental motions at nanosecond frequencies have been correlated with the bulk modulus of both synthetic polyesters and protective plant biopolymers from lime and tomato cutin as well as potato wound suberin,[28,64,66,67] providing a precedent for the use of ssNMR to establish structure-dynamics-function correlations in other biomacromolecular assemblies. For cutins and suberins, motions occurring at the spin-lock frequency in rotating-frame nuclear relaxation measurements have been proposed, in analogy with engineered polymers, to reflect the impact strength or toughness of biopolymer-based plant coverings.[22,28,66,68] Although prior assessments of microsecond motions have been limited by poor NMR sensitivity and nonexponential decays (for $T_{1\rho}(C)$) or averaging of values by spin diffusion (for $\langle T_{1\rho}(H)\rangle$),[71] the Lee−Goldburg (LG) spin-lock procedure used herein preserves site-specific information while allowing practical measurement of $T_{1\rho}(H)$s through the ^{13}Cs directly bound to the respective ^{1}H nuclei.[52] The distinct values observed via each carbon signal show variations for native (wild-type and FHT-RNAi) and wound periderms that all track the previously reported $\langle T_{1\rho}(C)\rangle$ trends for potato wound suberin.[28]

2. Suberized Cell Walls and Permeability Function in Native versus Wound Periderm Assemblies. As noted above, the biopolymers in native and wound periderm exhibit ^{13}C NMR spectra with comparable types of functional groups (Figure 1). However, the primarily polysaccharide alkoxy groups outnumber the $(CH_2)_n$ carbons for the polyester in wound periderm, whereas the aliphatic chain carbons appear dominant in spectra of the native suberized cell walls (Figure 2). Consequently, the wound periderm is rich in water-loving moieties as judged by the ratio of alkoxy to alkyl chain moieties (Figure 3A), a reasonable finding in light of its hundredfold larger permeability.[34] A sparse $(CH_2)_n$ population in the wound periderm could compromise hydrophobic interactions with waxes that are required to form a blend with good sealing performance, as also discussed below for the FHT-RNAi and CYP86A33-RNAi periderms.

With regard to the multiply bonded carbon-containing groups, our NMR spectra show that they outnumber the $(CH_2)_n$ groups in wound periderm, but the relative proportions are roughly reversed for native samples (Figure 3). This relative abundance of arene and alkene moieties in wound periderm is compatible with prior solid-state NMR and histological evidence that aromatic structures assemble prior to their aliphatic counterparts during suberization.[30,72] Though observation of a common set of aromatic resonances and similar CH/C ratios derived from the ^{13}C NMR spectra of native (Figure S2) and wound[9] periderms suggest comparable molecular organization of their suberins, thioacidolysis breakdown products[36] indicate that syringyl or sinapyl units are more dominant in wound tissues. The multiply bonded (aromatic) chemical groups are also retained to a greater degree in the undegraded residue from wound periderm (Figures 5A,B), suggesting they have fewer covalent (ester) attachments to the degradable aliphatic polyester groups, a greater fraction of nonester bonds to the cell walls, and a location within the macromolecular assembly that is inaccessible to the methanolysis reagent.

In addition to the compositional trends observed for the wound periderm, there are notable alterations in molecular flexibility that can be evaluated in site-specific and time scale-specific terms to gain insights into macromolecular architecture and periderm function. Compared with native wild-type and FHT-RNAi samples, polyester acyl chains in the wound periderm display augmented cooperative microsecond motions that facilitate efficient rotating-frame spin relaxation (shorter $T_{1\rho}(H)$ values), notably for the semicrystalline $(CH_2)_n$ groups (33 ppm; Figure 6). In wound periderm, the primarily polyester oxymethylene groups (62−64 ppm) and largely polysaccharide oxymethine groups (72 ppm) also show relatively enhanced local segmental nanosecond motions (shorter values of $T_1(C)$; Figure 6). The paucity of $(CH_2)_n$ groups produced by wound suberin thus results in formation of a macromolecular assembly for which only the most rigid subset of long-chain segments is "loosened", suggesting that anchoring constraints have become

less prevalent. For both groups of alkoxy moieties (62−64 and 72 ppm), restricted motion on both microsecond and nanosecond time scales can be attributed to contributions from polysaccharides or cross-linked aliphatic suberan constituents that are inaccessible to methanolysis. For wound periderms, in particular, alkoxy segmental motions are notably less constrained, again in accord with a model in which polyester−polysaccharide anchors are absent. These observations suggest that, in addition to sufficient $(CH_2)_n$ groups to form a hydrophobic seal with periderm waxes, a robust barrier to water transpiration requires the rigidity and organized suprastructure typical of native periderms.[34] The spin relaxation findings also underscore the importance of flexibility on two time scales and the distinct roles of polyester and polysaccharide constituents in determining plant periderm protective functions.

3. Recalcitrant Suberan Biopolymer Fraction. In analogy to the nonsaponifiable cutan biopolymers derived from plant cutins and soil organic matter,[21,73−75] we designate suberan as the insoluble residue that persists in transesterified plant suberins[12−14,33,76] because its covalent linkages are inaccessible or chemically unreactive with respect to the customary degradative reagents. Whereas a subset of cutans occur in conjunction with polysaccharides from the underlying cell walls, many of these materials have been identified as fatty acid esters and some depolymerization residues have been reported to possess ether, alcohol, carboxylic acid, epoxy, phenolic, or semicrystalline polyethylene functional groups.[21,73−75] For depolymerization-resistant suberans, such structural comparisons are complicated by differences in sample source, chemical treatment history, breakdown efficiency, and spectroscopic characterization methodology. For instance, the recalcitrant residues from chemical transesterification have been reported to comprise 50−90% by weight of the starting periderm tissues for potatoes and birch bark.[12−14,33] Thus, in addition to arguing for caution in the analysis of soluble breakdown product profiles, the partial extent of depolymerization for suberized plant cell walls limits the scope of our proposals regarding suberan molecular structure.

The solid-state ^{13}C NMR spectra of Figures 5 and S5 show that undegraded residues from all potato periderm samples studied herein are composed predominantly of polysaccharides, as reported previously for both native[13,33] and wound[12] materials. Except for FHT-RNAi periderm, the ssNMR spectra evidence small proportions of retained aliphatic chain moieties, suggesting that the amount and chemical composition of aliphatic ester monomer constituents can be determined reliably for potato periderm from their respective soluble depolymerization product mixtures. The depolymerization left residues that show significant ^{13}C NMR spectral contributions from ester or uronic acid carboxyl groups (∼172 ppm), but our failure to observe commensurate $(CH_2)_n$ and COO removal strongly suggests retention of suberans that are structurally distinct from the polyester structure usually attributed to suberin. Although a glycerol-based polyester model[5] has been advanced for *Betula nigra* suberan,[14] the modest extent of suberin breakdown and the presence of dominant polysaccharide resonances in the same 60−80 ppm alkoxy region of the CPMAS ^{13}C NMR spectrum make this hypothesis difficult to evaluate.

A more comprehensive molecular specification of the recalcitrant fractions is possible by considering the CYP86A33-RNAi and FHT-RNAi periderms, which represent two contrasting profiles of saponifiable aliphatics, ultrastructural organization, and ssNMR signature. CYP86A33-RNAi periderm shows a 43% reduction ($\mu g\ mg^{-1}$) in soluble transesterification products, less organized suberin lamellae, and a deficiency in the major bifunctional monomers (C18:1 ω-hydroxyacid and α,ω-diacid).[44] However, Figure 5 shows that the CYP86A33-RNAi recalcitrant residue retains similar (small) proportions of aliphatic groups to wild-type, suggesting that they have a common aliphatic suberan polymer that coexists with the saponifiable material within the intact suberized cell walls.[14]

Conversely, the FHT-RNAi periderm has a knocked-down capacity to synthesize alkyl ferulates but retains the lamellar organization of its suberized cell walls.[38] As compared with the wild-type, this periderm shows 89% reductions ($\mu g\ mg^{-1}$) in both esterified ferulic acid and C18:1 ω-hydroxyacid,[38] which are found together as an esterified soluble product upon partial transesterification of the wild-type potato suberin.[10] With this esterification suppressed genetically, a finding of increased conjugated polyamines has suggested redirection of the unesterified free feruloyl-CoA pool to soluble phenolics,[38] though the fate of the C18:1 ω-hydroxyacid is uncertain. Figure 5 demonstrates a striking increase in the nonsaponifiable aliphatic and aromatic fractions for FHT-RNAi as compared with wild-type and CYP86A33-RNAi. The former periderm's ferulic acid processing could produce a more heavily cross-linked aromatic domain (see next section) that is thus less accessible to depolymerization. Alternatively or additionally, ω-hydroxyacid could be incorporated in nonester forms that leave it behind as aliphatic FHT-RNAi suberan after the transesterification treatment. The proposal of ferulic acid reprocessing is also consistent with the elevated aromatic/$(CH_2)_n$ ratio displayed in Figure 4 for the intact suberin macromolecular cell-wall assembly.

Taking into account these several considerations, our findings support the hypothesis that suberan is a distinct biopolymer that coexists with suberin. In potato periderm this fraction can be produced even if C18:1 ω-hydroxyacid and α,ω-diacid levels are compromised by RNAi silencing, suggesting that other synthesized compounds could be incorporated into the suberan macromolecular assembly. Our results also suggest that ferulate esters are not required for suberan formation, but the undegraded FHT-RNAi residue displays a distinctive chemical structure. Nonetheless, these facts do not preclude the possibility that suberan is derived from suberin, as reported for cutan and cutin.[77,78] Finally, our results suggest that suberan is not directly related to the lamellar organization of suberin, and therefore, other structural or enzymatic factors are likely required to establish the lamellae.[6]

4. Molecular Basis for Physicochemical Properties of Genetically Modified Suberin Macromolecular Assemblies. When pulled to the limit of their strength, the periderm membranes with genetically modified suberins behaved differently from each other. In general, the mechanical properties of macromolecules can be related to the length, flexibility, stereoregularity, and cross-linking of the polymer chains, while transport properties such as diffusivity depend on how rapidly molecules can move through the polymer matrix.[79]

The StKCS6-deficient periderm has a similar total transesterified lipid amount and composition to wild-type and exhibits the typical ordered periderm lamellae, though it exhibits modestly shorter carbon lengths as expected and increased permeability. Moreover, ssNMR analysis of the intact

polymer (Figures 1, 2, and 4) and the undegraded residue (Figure 5) revealed similar molecular composition and architecture to the wild-type. Our measurements of tensile stress creep deformation for the StKCS6-RNAi membranes (Figure 7) did not reveal differences from wild-type.

In contrast, the CYP86A33-RNAi periderm exhibited lower tensile strength and higher plasticity than the wild-type periderm (Figure 7). The much lower amounts of transesterified aliphatic suberin that characterize this periderm include compositional profiles with significantly larger proportions of monofunctional lipids (fatty acids and fatty alcohols) in relation to bifunctional lipids (ω-hydroxyacids and α,ω-diacids) and glycerol (Table 1). Given the completeness of aliphatic chain removal evidenced by the ssNMR spectra of Figure 5, this monomer composition can be interpreted to imply a greatly reduced degree of cross-linking capacity within the polyester matrix[6,44] and is supported by the enhanced fraction of mobile $(CH_2)_n$ groups displayed in Figure 4D. The reduction in cross-linking capability could also impart a less regular internal organization to the polymer composite, as exemplified by the uneven distribution of electron-dense and electron-translucent material in the suberin wall.[44] In turn, diminished polymer−polymer interactions could account for the lower tensile strength and grained appearance of ruptured CYP86A33-RNAi cell walls (Figure 7F).

The shift in hydrophilic−hydrophobic balance for CYP86A33-RNAi periderms, established by ssNMR results showing a lowered proportion of aliphatic chains in relation to alkoxy and carboxyl functional groups (Figure 4A,B), gives this periderm more affinity and capacity for interactions with water. The expected reductions in hydrophobic chain−chain interactions are consistent with observation of a slightly elevated fraction of mobile $(CH_2)_n$ groups (Figure 4D). These properties are both compatible with the 3.5-fold larger permeability observed for the CYP86A33-RNAi periderm[44] and are reasonable because a substandard chain-methylene population could compromise formation of a polyester-wax seal. Although the aromatic carbon ssNMR spectral features are similar for CYP86A33-RNAi and wild-type periderms, the genetically modified periderm shows an enhanced ratio of aromatics to aliphatic chains (Figure 4C). Considering that the covalent anchoring and cross-linking of suberin to cell walls are attributed to the aromatic groups,[4,9] the CYP86A33-RNAi periderms might be expected to recover their dimensional integrity after stress relief, whereas in fact we observe a more plastic behavior. Thus, we attribute the viscoelastic properties of this periderm to the impaired aliphatic domain organization, following analogous hypotheses advanced to rationalize plastic contributions to extensibility in tomato cuticular materials[80] and compositionally linked variations in the elasticity and relaxation properties of cork stoppers.[3]

Finally, the FHT-RNAi periderm showed lower tensile strength but greater stiffness than wild-type (Figure 7). This modified biopolymer membrane is thicker, more brittle, prone to cracks, russeted in appearance, and 15-fold more permeable to water compared with the wild-type. Moreover, FHT-RNAi carries a 62% smaller total suberin lipid load ($\mu g\ mg^{-1}$) compared to the wild-type periderm (Table 1).[38] It should be noted that, although ∼89% ($\mu g\ mg^{-1}$) fewer ferulate esters are released as soluble depolymerization products (as expected due to FHT silencing), new related conjugated polyamine compounds (feruloyl and caffeoyl putrescine, feruloyltyramine and octopamine) are produced.[38] Thus, we surmise that ferulic acid is redirected to other biosynthetic pathways so that the suberized cell wall is "rebuilt" as a stiffer periderm that exhibits increased permeability and lower tensile strength. This hypothesis is supported by an elevated aromatic/$(CH_2)_n$ ratio (Figure 4) and less efficient μs and ns motions (Figure 6), but the likely incorporation of new types of polyphenolics that are uniquely retained in the aromatic fraction of the FHT-RNAi undegraded residue (Figure 5) makes it unwise to attempt direct comparisons of these group ratios with other periderms. Conjugated polyamines are thought to serve many roles, including cell-wall reinforcement through the formation of ferulic acid bridges[81] that have been related to the increase in thermal stability of the cell wall[82,83] and to changes in texture and stiffness of plant tissues.[84,85] Increases in feruloyl amides have been correlated with lesion formation in common scab-infected potato tubers,[86,87] which have heavier and more brittle skin similar to that of FHT-RNAi potatoes. Besides, insufficient flexibility has been proposed to promote cracking of the polymeric veneer of fruit cuticles that increases water permeability.[22,66] Viewed together, it seems reasonable to attribute the greater stiffness and more brittle texture of the FHT-RNAi periderm to the redirection of ferulic acid moieties so that ordered stacking is favored rather than esterification to alkyl chains. Although the chain $(CH_2)_n$ groups exhibit similar nanosecond motions to wild-type periderm (Figure 6), a greater fraction of them are "liquidlike" (Figure 4D) and presumably less tethered by other cell-wall constituents. These observations underscore the point that anomalous functionality (e.g., waterproofing ability or microfissuring susceptibility) is unlikely to reside entirely in the suberin properties but must also reflect intercomponent interactions with waxes and cell walls.

The elevated $(CHO + CH_2O + CH_3O)/(CH_2)_n$ ratio (Figure 4A) and enhanced hydrogen-bonded OH stretching absorbance (Figure S4) both indicate a more hydrophilic FHT-RNAi periderm that can facilitate water transpiration, but as for the aromatic/$(CH_2)_n$ ratio, the NMR-based correlation is qualitative: a similar ratio is found for the CYP86A33-RNAi periderm even though it shows only a 3.5-fold increase in permeability. The correspondence between sparse but disproportionately flexible chain methylenes (Figure 6) and facile water transpiration in the FHT-RNAi assembly can be explained if chain packing is disrupted by oxygen-linked branches, though steric hindrance could limit the observation of the corresponding transesterifcation products. Conversely, the relative decrease in suberin chain methylenes by 62% ($\mu g\ mg^{-1}$), which is accompanied by an unremarkable wax content (∼5.4 $\mu g\ mg^{-1}$),[38] can produce a numerical mismatch between their respective chains that undercuts the hydrophobic association and motional restriction typical of a robust cuticular waterproofing layer.[66] Given that esterification to ferulic acid is dramatically attenuated in the FHT-RNAi periderm, the potential long-chain aliphatic "partners" should be more loosely anchored in the modified suberin assembly, highly mobile (Figure 4D), and present in a chemical form that is less susceptible to degradative breakdown (Figure 5).

CONCLUSIONS

In summary, a coordinated set of ssNMR, FT-IR, and tensile strength measurements has provided atomic-level insights into the structure−dynamics−function relationships of an agriculturally important biomacromolecular assembly and has offered guidance for the engineering of other polymer-based water-

proofing materials. Wound-healing suberized potato cell walls, which are 2 orders of magnitude more permeable to water than native periderms, are found to have a strikingly reduced proportion of alkyl chain moieties that enhance their hydrophilic−hydrophobic balance, an aromatic domain more resistant to chemical degradation, and more flexible molecular groupings that could reflect a less organized periderm supramolecular structure. Genetically modified potato periderms provide a means to examine the structural and functional consequences of designed metabolic alterations, wherein a comprehensive view is obtained by coordinating information from intact periderms, soluble depolymerization products, and undegraded residues. For StKCS6-RNAi periderms in which chain elongation is modestly diminished, these studies reveal similar molecular composition, mechanical performance, and permeability to wild-type. In CYP86A33-RNAi periderms for which terminal fatty acid hydroxylation and cross-linking capacity are knocked down, the results are a greater fraction of mobile alkyl chains, loss of lamellar structure, and enhanced permeability. Moreover, downregulation of ferulate ester formation in FHT-RNAi potatoes remodels the periderm with more flexible aliphatic chains but abundant aromatic constituents that are resistant to transesterifcation; this modification also attenuates cooperative motions at the junctures between hydroxyfatty acid units and produces a periderm that is mechanically compromised and highly permeable to water. In terms of mechanical performance, changes in the aliphatic domain impacted viscoelastic properties, whereas changes in the aromatics controlled mechanical strength and resiliency.

Overall, the architecture of suberin with respect to associated cell-wall polymers and waxes gives the potato periderm its unique strength, elasticity, and impermeability. The structure of each aliphatic and aromatic suberin domain, as well as networked interactions among acyl chains, aromatic rings, polysaccharides, and waxy coatings, is necessary to achieve the micromechanical and protective properties of this periderm biopolymer assembly. As demonstrated herein, both structure and function are responsive to whether native or wound periderms are synthesized by the plant and if key genes are suppressed in the native periderms. A delicate balance among these compositional, supramolecular, and motional properties of the suberized cell walls is essential to maintain periderm functionality as a barrier to water transpiration with excellent mechanical integrity.

■ ASSOCIATED CONTENT

Ⓢ Supporting Information

CPMAS ^{13}C NMR (150 MHz) spectra of native and wound periderm replicates; 150 MHz CPMAS ^{13}C NMR spectra of wild-type and genetically modified native periderms obtained with delayed decoupling periods of 0−40 μs; 150 MHz ^{13}C CPMAS NMR spectra of genetically modified native periderm replicates from two independent lines; FT-IR spectra of native and genetically modified potato periderms; 150 MHz DPMAS ^{13}C NMR of wild-type and genetically modified native periderms in comparison with their undegraded solid residues after methanolysis; rotating-frame proton spin relaxation times measured with a spin-lock field of 106 kHz; aliphatic suberin monomeric composition in native wild-type and genetically modified periderms; ^{13}C NMR chemical shift assignments for potato periderm samples. This material is available free of charge via the Internet at http://pubs.acs.org.

■ AUTHOR INFORMATION

Corresponding Author

*Tel.: +1-212-650-8916. Fax: +1-212-650-8719. E-mail: rstark@ccny.cuny.edu.

Author Contributions

†These authors contributed equally to this work (O.S. and S.C.).

Notes

The authors declare no competing financial interest.

■ ACKNOWLEDGMENTS

This research was supported by grants from the U.S. National Science Foundation (MCB-0843627) and the Ministerio de Innovación y Ciencia (AGL2009-13745). O.S. gratefully acknowledges mobility grant (JC2010-0147) from the Ministerio de Educación. The NMR resources were supported by The City College of New York and the CUNY Institute for Macromolecular Assemblies, with additional infrastructural support provided by NIH 2G12RR03060 from the National Center for Research Resources and 8G12MD007603 from the National Institute on Minority Health and Health Disparities. We thank Dr. Hsin Wang for valuable technical support in connection with the solid-state NMR experiments, Prof. Teresa Bandosz (CUNY) and the Chemistry Department (UdG) for access to the ATR-IR equipment, and Dr. Joan Pere Lopez and Mrs. Carme Carulla for technical support of mechanical and SEM experiments, respectively. We also are very grateful to Mrs. Sara Gomez for her valuable work in potato cultivation.

■ REFERENCES

(1) Esau, K. *Plant Anatomy*, 2nd ed.; Wiley: New York, 1965.
(2) Silva, S. P.; Sabino, M. A.; Fernandes, E. M.; Correlo, V. M.; Boesel, L. F.; Reis, R. L. *Int. Mater. Rev.* **2005**, *50*, 345−365.
(3) Pereira, H. *BioResources* **2013**, *8*, 2246−2256.
(4) Bernards, M. A. *Can. J. Bot.* **2002**, *80*, 227−240.
(5) Graca, J.; Santos, S. *Macromol. Biosci.* **2007**, *7*, 128−135.
(6) Pollard, M.; Beisson, F.; Li, Y.; Ohlrogge, J. B. *Trends Plant Sci.* **2008**, *13*, 236−246.
(7) Beisson, F.; Li-Beisson, Y.; Pollard, M. *Curr. Opin. Plant Biol.* **2012**, *15*, 329−37.
(8) Bernards, M. A.; Lopez, M. L.; Zajicek, J.; Lewis, N. G. *J. Biol. Chem.* **1995**, *270*, 7382−7386.
(9) Yan, B.; Stark, R. E. *J. Agric. Food Chem.* **2000**, *48*, 3298−3304.
(10) Graca, J.; Pereira, H. *Biomacromolecules* **2000**, *1*, 519−522.
(11) Dean, B. B.; Kolattukudy, P. E.; Davis, R. W. *Plant Physiol.* **1977**, *59*, 1008−1010.
(12) Stark, R. E.; Zlotnik-Mazori, T.; Ferrantello, L. M.; Garbow, J. R. *ACS Symp. Ser.* **1989**, *399*, 214−229.
(13) Järvinen, R.; Silvestre, A. J. D.; Gil, A. M.; Kallio, H. *J. Food Comp. Anal.* **2011**, *24*, 334−345.
(14) Turner, J. W.; Hartman, B. E.; Hatcher, P. G. *Org. Geochem.* **2013**, *57*, 41−53.
(15) Ranathunge, K.; Schreiber, L.; Franke, R. *Plant Sci.* **2011**, *180*, 399−413.
(16) Zlotnik-Mazori, T.; Stark, R. E. *Macromolecules* **1988**, *21*, 2412−2417.
(17) Stark, R. E.; Yan, B.; Ray, A. K.; Chen, Z.; Fang, X.; Garbow, J. R. *Solid State Nucl. Magn. Reson.* **2000**, *16*, 37−45.
(18) Serra, O.; Chatterjee, S.; Huang, W.; Stark, R. E. *Plant Sci.* **2012**, *195*, 120−4.
(19) Garbow, J. R.; Stark, R. E. *Macromolecules* **1990**, *23*, 2814−2819.
(20) Deshmukh, A. P.; Simpson, A. J.; Hatcher, P. G. *Phytochemistry* **2003**, *64*, 1163−1170.
(21) Deshmukh, A. P.; Simpson, A. J.; Hadad, C. M.; Hatcher, P. G. *Org. Geochem.* **2005**, *36*, 1072−1085.

(22) Stark, R. E.; Yan, B.; Stanley-Fernandez, S. M. *Phytochemistry* **2008**, *69*, 2689−95.
(23) Pascoal Neto, C.; Rocha, J.; Gil, A.; Cordeiro, N.; Esculcas, A. P.; Rocha, S.; Delgadillo, I.; Jesus, J. D. P.; De Correia, A. J. F. *Solid State NMR* **1995**, *4*, 143−151.
(24) Gil, A. M.; Lopes, M.; Rocha, J.; Pascoal Neto, C. *Int. J. Biol. Macromol.* **1997**, *20*, 293−305.
(25) Lopes, M. H.; Gil, A. M.; Silvestre, A. J. D.; Neto, C. P. *J. Agric. Food Chem.* **2000**, *48*, 383−391.
(26) Rocha, S. M.; Goodfellow, B. J.; Delgadillo, I.; Pascoal Neto, C.; Gil, A. M. *Int. J. Biol. Macromol.* **2001**, *28*, 107−19.
(27) Garbow, J. R.; Ferrantello, L. M.; Stark, R. E. *Plant Physiol.* **1989**, *90*, 783−787.
(28) Stark, R.; Garbow, J. *Macromolecules* **1992**, *25*, 149−154.
(29) Pacchiano, R. A.; Sohn, W.; Chlanda, V. L.; Garbow, J. R.; Stark, R. E. *J. Agric. Food Chem.* **1993**, *41*, 78−83.
(30) Stark, R. E.; Sohn, W.; Pacchiano, J. R. A.; Al-Bashir, M.; Garbow, J. R. *Plant Physiol.* **1994**, *104*, 527−533.
(31) Bernards, M. A.; Lewis, N. G. *Phytochemistry* **1998**, *47*, 915−933.
(32) Mattinen, M.-L.; Filpponen, I.; Järvinen, R.; Li, B.; Kallio, H.; Lehtinen, P.; Argyropoulos, D. *J. Agric. Food Chem.* **2009**, *57*, 9747−53.
(33) Järvinen, R.; Silvestre, A. J. D.; Holopainen, U.; Kaimainen, M.; Nyyssölä, A.; Gil, A. M.; Pascoal Neto, C.; Lehtinen, P.; Buchert, J.; Kallio, H. *J. Agric. Food Chem.* **2009**, *57*, 9016−27.
(34) Schreiber, L.; Franke, R.; Hartmann, K. *Planta* **2005**, *220*, 520−30.
(35) Sabba, R. P.; Lulai, E. C. *Ann. Bot.* **2002**, *90*, 1−10.
(36) Lapierre, C.; Pollet, B.; Negrel, J. *Phytochemistry* **1996**, *42*, 949−953.
(37) Serra, O.; Soler, M.; Hohn, C.; Franke, R.; Schreiber, L.; Prat, S.; Molinas, M.; Figueras, M. *J. Exp. Bot.* **2009**, *60*, 697−707.
(38) Serra, O.; Hohn, C.; Franke, R.; Prat, S.; Molinas, M.; Figueras, M. *Plant J.* **2010**, *62*, 277−90.
(39) Hammes, K.; Smernik, R. J.; Skjemstad, J. O.; Herzog, A.; Vogt, U. F.; Schmidt, M. W. I. *Org. Geochem.* **2006**, *37*, 1629−1633.
(40) Franke, R.; Briesen, I.; Wojciechowski, T.; Faust, A.; Yephremov, A.; Nawrath, C.; Schreiber, L. *Phytochemistry* **2005**, *66*, 2643−58.
(41) Yang, W. L.; Bernards, M. A. *Metabolomics* **2007**, *3*, 147−159.
(42) Kolattukudy, P. E.; Agrawal, V. P. *Lipids* **1974**, *9*, 682−691.
(43) Zeier, J.; Schreiber, L. *Planta* **1998**, *206*, 349−361.
(44) Serra, O.; Soler, M.; Hohn, C.; Sauveplane, V.; Pinot, F.; Franke, R.; Schreiber, L.; Prat, S.; Molinas, M.; Figueras, M. *Plant Physiol.* **2009**, *149*, 1050−60.
(45) Matas, A. J.; Yeats, T. H.; Buda, G. J.; Zheng, Y.; Chatterjee, S.; Tohge, T.; Ponnala, L.; Adato, A.; Aharoni, A.; Stark, R. E.; Fernie, A. R.; Fei, Z.; Giovannoni, J. J.; Rose, J. K. C. *Plant Cell* **2011**, *23*, 3893−910.
(46) Opella, S. J.; Frey, M. H.; Cross, T. A. *J. Am. Chem. Soc.* **1979**, *101*, 5854−5857.
(47) Harbison, G. S.; Mulder, P. P. J.; Pardoen, H.; Lugtenburg, J.; Herzfeld, J.; Griffin, R. G. *J. Am. Chem. Soc.* **1985**, *107*, 4809−4816.
(48) Fung, B. M.; Khitrin, A. K.; Ermolaev, K. *J. Magn. Reson.* **2000**, *142*, 97−101.
(49) Chatterjee, S.; Sarkar, S.; Oktawiec, J.; Mao, Z.; Niitsoo, O.; Stark, R. E. *J. Visualized Exp.* **2012**, 1−7−e529.
(50) Chatterjee, S.; Santos, F.; Abiven, S.; Itin, B.; Stark, R. E.; Bird, J. A. *Org. Geochem.* **2012**, *51*, 35−44.
(51) Stejskal, E. O.; Schaefer, J.; Steger, T. R. *Faraday Symp. Chem. Soc.* **1979**, *13*, 56−62.
(52) Domain, M. C. I. C.; Huster, D.; Xiao, L.; Hong, M. *Biochemistry* **2001**, *40*, 7662−7674.
(53) Dick-Pérez, M.; Zhang, Y.; Hayes, J.; Salazar, A.; Zabotina, O. A.; Hong, M. *Biochemistry* **2011**, *50*, 989−1000.
(54) Ladizhansky, V.; Vega, S. *J. Chem. Phys.* **2000**, *112*, 7158−7168.
(55) Akasaka, K. *J. Chem. Phys.* **1983**, *78*, 3567−3572.
(56) Torchia, D. A. *J. Magn. Reson.* **1978**, *30*, 613−616.
(57) Hediger, S.; Emsley, L.; Fischer, M. *Carbohydr. Res.* **1999**, *322*, 102−112.
(58) Masuda, K.; Tabata, S.; Sakata, Y.; Hayase, T.; Yonemochi, E.; Terada, K. *Pharm. Res.* **2005**, *22*, 797−805.
(59) Zeier, J.; Schreiber, L. *Planta* **1999**, *209*, 537−42.
(60) Kolodziejski, W.; Klinowski, J. *Chem. Rev.* **2002**, *102*, 613−28.
(61) Isaacson, T.; Kosma, D. K.; Matas, A. J.; Buda, G. J.; He, Y.; Yu, B.; Pravitasari, A.; Batteas, J. D.; Stark, R. E.; Jenks, M. A.; Rose, J. K. C. *Plant J.* **2009**, *60*, 363−77.
(62) Sinitsya, A.; Copiková, J.; Pavliková, H. *J. Carbohydr. Chem.* **1998**, *17*, 279−292.
(63) Yan, B.; Stark, R. E. *Macromolecules* **1998**, *31*, 2600−2605.
(64) Round, A. N.; Yan, B.; Dang, S.; Estephan, R.; Stark, R. E.; Batteas, J. D. *Biophys. J.* **2000**, *79*, 2761−7.
(65) Stark, R. E.; Tian, S. In *Annual Plant Reviews. Biology of the Plant Cuticle*; Riederer, M.; Muller, C., Eds.; Blackwell Publishing Co.: Oxford, U.K., 2008; pp 126−144.
(66) Garbow, J. R.; Stark, R. E. *Macromolecules* **1990**, *23*, 2814−2819.
(67) Bovey, F. A.; Jelinski, L. W. *J. Phys. Chem.* **1985**, *89*, 571−583.
(68) Schaefer, J.; Stejskal, E. O.; Buchdahl, R. *Macromolecules* **1977**, *10*, 384−405.
(69) Hatfield, G. R.; Maciel, G. E.; Erbatur, O.; Erbatur, G. *Anal. Chem.* **1987**, *59*, 172−179.
(70) North, A. M. *Molecular Behavior and the Development of Polymeric Materials*; Ledwith, A., North, A. M., Eds.; Wiley: New York, 1975.
(71) Schaefer, J.; Stejskal, E. O. *Top. Carbon-13 NMR Spectrosc.* **1979**, *3*, 283−324.
(72) Lulai, E. C.; Corsini, D. L. *Physiol. Mol. Plant Pathol.* **1998**, *53*, 209−222.
(73) Nip, M.; Tegelaar, E. W.; de Leeuw, J. W.; Schenck, P. A.; Holloway, P. J. *Naturwissenschaften* **1986**, *73*, 579−585.
(74) Villena, J. F.; Dominguez, E.; Stewart, D.; Heredia, A. *Planta* **1999**, *208*, 181−187.
(75) Sachleben, J. R.; Chefetz, B.; Deshmukh, A. P.; Hatcher, P. G. *Environ. Sci. Technol.* **2004**, *38*, 4369−4376.
(76) Tegelaar, E.; Hollman, G.; Van Der Vegt, P.; de Leeuw, J. W.; Holloway, P. *Org. Geochem.* **1995**, *23*, 239−250.
(77) Gupta, N. S.; Michels, R.; Briggs, D. E. G.; Collinson, M. E.; Evershed, R. P.; Pancost, R. D. *Org. Geochem.* **2007**, *38*, 28−36.
(78) Gupta, N. S.; Briggs, D. E. G.; Collinson, M. E.; Evershed, R. P.; Michels, R.; Jack, K. S.; Pancost, R. D. *Org. Geochem.* **2007**, *38*, 499−522.
(79) Pollard, M.; Beisson, F.; Li, Y.; Ohlrogge, J. *Trends Plant Sci.* **2008**, *13*, 236−246.
(80) Petracek, P. D.; Bukovac, M. J. *Plant Physiol.* **1995**, *109*, 675−679.
(81) Matsuda, F.; Morino, K.; Ano, R.; Kuzawa, M.; Wakasa, K.; Miyagawa, H. *Plant Cell Physiol.* **2005**, *46*, 454−66.
(82) Liyama, K.; Lam, T.; Stone, B. A. *Plant Physiol.* **1994**, *104*, 315−320.
(83) Parker, C. C.; Parker, M. L.; Smith, A. C.; Waldron, K. W. *J. Agric. Food Chem.* **2001**, *41*, 4364−4371.
(84) Rodríguez-Arcos, R. C.; Smith, A. C.; Waldron, K. W. *J. Agric. Food Chem.* **2004**, *52*, 4740−50.
(85) De O Buanafina, M. M. *Mol. Plant* **2009**, *2*, 861−72.
(86) King, R. R.; Calhoun, L. A. *Phytochemistry* **2005**, *66*, 2468−73.
(87) King, R. R.; Calhoun, L. A. *Phytochemistry* **2010**, *71*, 2187−9.